Derivation of plastic stress–strain relationship from ball indentations: Examination of strain definition and pileup effect

Jeong-Hoon Ahn and Dongil Kwon
School of Materials Science and Engineering, Seoul National University, Seoul 151-742, Korea

(Received 27 December 2000; accepted 21 August 2001)

The ball indentation technique has the potential to be an excellent substitute for a standard tensile test, especially in the case of small specimens or property-gradient materials such as welds. In our study, the true stress–true strain relationships of steels with different work-hardening exponents (0.1–0.3) were derived from ball indentations. Four kinds of strain definitions in indentation were attempted: $0.2\sin\gamma$, $0.4h_c/a$, $\ln[2/(1+\cos\gamma)]$, and $0.1\tan\gamma$. Here, γ is the contact angle between the indenter and the specimen, h_c is the contact depth, and a is the contact radius. Through comparison with the standard data measured by uniaxial tensile testing, the best strain definition was determined to be $0.1\tan\gamma$. This new definition of strain, in which $\tan\gamma$ means the shear strain at contact edge, reflected effectively the work-hardening characteristics. In addition, the effects of pileup or sink-in were considered in determining the real contact between the indenter and the specimen from the indentation load–depth curve. The work-hardening exponent was found to be a main factor affecting the pileup/sink-in phenomena of various steels. These phenomena influenced markedly the absolute values of strain and stress in indentation by making the simple traditional relationship $P_m/\sigma_R \approx 3$ valid for the fully plastic regime.

I. INTRODUCTION

The evaluation of mechanical properties of structural steels plays an important role in diagnosing the material degradation under high temperature and pressure. This demands property-evaluation techniques that are simple, easy, nondestructive, and suitable for localized weak zones such as welds and heat-affected zones. One of these techniques, the continuous indentation test, records the indentation depth continuously with indentation load. Compared with conventional hardness tests, it offers us complete information during indentation loading and unloading through analysis of the measured indentation load–depth curve.

The representative mechanical properties evaluated from the indentation load–depth curve are hardness and elastic modulus. In continuous indentation tests, hardness is usually defined as the mean contact pressure between the indenter and the specimen. While the residual imprint is observed as a contact area in conventional hardness tests, the projected contact area at maximum load must be calculated from the indentation load–depth curve. This overcomes one disadvantage of conventional hardness tests: hardness values for highly elastic materials such as rubber are too high.

It is noted that the interpretation of experimental results has not been standardized because of complex stress fields beneath the indenter. Moreover, the definition of hardness as mean contact pressure does not yield a basic material property for indicating the material strength.[1,2] In other words, hardness is affected by the elastic and plastic properties of material, the indenter shape, and partially by the experimental procedures and the surface condition of specimen. Accordingly, many attempts have been made to get more intrinsic properties from indentation tests such as yield[3–7] or tensile strength[8] and even flow properties[9–14] of materials.

This paper describes the derivation of the true stress–true strain relationship from the indentation load–depth curve measured by the ball indentation technique. To determine the real contact between the indenter and the specimen from the indentation load–depth curve, both the elastic deflection and the pileup or sink-in are taken into account. Also, the effects of pileup or sink-in on deriving the stress–strain relationship are discussed. Four kinds of strain definitions in indentation were examined for AISI1025, SA106, SA213, SA508, SM50, and thermomechanical-control-process (TMCP) steels with different work-hardening characteristics. By comparing the true stress–true strain curve derived from ball

indentations with those measured directly by the uniaxial tensile test, we made a new definition of strain and investigated the ratio of mean contact pressure to representative stress in indentation.

II. THEORETICAL ANALYSIS

Material response during indentation depends on the indenter shape. For a ball indenter, it is divided into the three regimes[3,9,11] shown in Fig. 1: elastic, elastic–plastic, and fully plastic. As the ball indenter penetrates into the specimen, the average strain beneath the indenter increases, as does the mean contact pressure. This increase makes it possible to derive the flow properties of the material by the ball indentation technique. On the other hand, for an indenter with geometrical similarity such as the Vickers indenter, the average strain and the mean contact pressure will be constant regardless of indentation depth if the effect of tip blunting can be ignored.

To establish the modeling of deriving the true stress–true strain relationship from ball indentations, the real contact between the indenter and the specimen will be determined from the indentation load–depth curve by considering both the elastic deflection and the pileup or sink-in. Then the representative strain and stress in indentation will be defined in terms of the obtained indentation contact parameters, i.e., contact depth h_c, contact radius a, and/or contact angle γ between the indenter and the specimen.

A. Analysis of indentation load–depth curve

The contact depth h_c between the indenter and the specimen at a certain load has usually been obtained by calculating the elastic deflection depth from the unloading curve:[15,16]

$$h_c^* = h_{max} - h_d \quad , \tag{1}$$

where h_{max} is the maximum indentation depth, h_d is the elastic deflection depth, and superscript (*) means that the effects of pileup or sink-in are not included. This relation is, however, not true for real materials showing the pileup or sink-in around indentation. Accordingly, it should be modified as

$$h_c = h_{max} - h_d + h_{p/s} \quad , \tag{2}$$

where $h_{p/s}$ means the change of contact depth due to pileup or sink-in.

The elastic deflection depth h_d in Eqs. (1) and (2) can be obtained by analyzing the unloading curve, which corresponds to elastic recovery during unloading. For the two extreme cases of perfectly elastic response and perfectly plastic response, h_d is obtained as follows. In the case of perfectly elastic response during ball indentation, shown in Fig. 2(a), there is no residual imprint after unloading and h_c equals ½ of h_{max} for a rigid indenter.[17] In other words, h_d equals ½ of h_{max}, and there is no pileup or sink-in. On the contrary, in the case of perfectly plastic response, shown in Fig. 2(c), there is no elastic deflection and the effects of pileup or sink-in must be included.

From the above consideration, it is seen that both the elastic deflection and the pileup or sink-in must be taken into account in determining the contact between the indenter and the specimen for real materials showing elastic–plastic response during indentation. The indentation load–depth curve is schematically shown in Fig. 2(b). In this curve, h_d is calculated by analyzing the unloading curve, whose initial slope is the stiffness S. By extrapolating this tangent line to zero load, the intercept depth h_i is defined. If there is no change in contact area during unloading, as occurs in flat punching, h_d will be h_{max}–h_i.[15] If the shape of indenter is taken into account, h_d will be obtained as $h_d = \omega\,(h_{max} - h_i)$.[16] This relation is derived from Sneddon's analysis[17] for a rigid indenter, and ω is a constant dependent on the indenter shape: 1 for a flat punch, 0.72 for a conical indenter, and 0.75 for a paraboloid of revolution.

The pileup or sink-in behavior around indentation alters the actual contact area.[14,18,19] If pileup occurs, the actual contact area will be larger than expected, and if sink-in occurs, the actual contact area will be smaller than expected. It is well established that the extent of this pileup/sink-in is determined by a dimensionless constant c for metals with low yield strain.[19]

$$c^2 = \frac{a^2}{a^{*2}} = \tfrac{5}{2}\,\frac{(2-n)}{(4+n)} \quad , \tag{3}$$

where a is the contact radius, a^* is the contact radius without considering the pileup or sink-in, and n is the work-hardening exponent of material. This equation is based on nonlinear elasticity theory and it was verified by finite element results. From this equation, it is inferred that the dominant factor affecting the shape and size of plastic zone during indentation for metals is related to the work-hardening characteristics. In detail, if the plastic zone beneath the indenter is large for a small n, the surrounding elastic zone cannot afford to accommodate the volume change due to the indenter penetration, so pileup will occur.

Using the geometrical relationship $a^{*2} = 2Rh_c^* - h_c^{*2}$ for ball indentations, the following equation can be established to determine the real contact between the indenter and the specimen from indentation load–depth curve.

$$a^2 = \tfrac{5}{2}\,\frac{(2-n)}{(4+n)}\,(2Rh_c^* - h_c^{*2}) \quad , \tag{4}$$

where R is the indenter radius. This equation means that the prediction of unknown n or another parameter related to pileup or sink-in is necessary to determine the actual contact radius from the measured indentation load–depth curve. In our study, this parameter will be determined using the model proposed in the following section and discussed later.

B. Derivation of true stress–true strain curve

Looking in detail at the three regimes occurring during ball indentation, the mean contact pressure increases as follows.[3] For the initial elastic regime, the mean contact pressure increases linearly with the square root of the indentation load. When the mean contact pressure reaches the elastic limit, the plastic zone will develop beneath the indenter as shown in Fig. 1. In the elastic–plastic regime, the mean contact pressure increases gradually. After the plastic zone expands to the surface of specimen, the mean contact pressure increases slightly due to work-hardening characteristics. This increase makes it possible to derive the plastic flow properties of material in the fully plastic regime.

When we usually define the stress or strain in indentation, its value does not mean a certain value at a specific point but an averaged value beneath the indenter. Work[14] done by finite element analysis is an exception. So, the terms of representative strain and representative stress, ϵ_R and σ_R, are used in our study as an averaged true strain and true stress beneath the indenter, respectively.

With the indentation parameters obtained from indentation load–depth curve in the previous section, ϵ_R can be defined in various ways. First, ϵ_R has usually been defined as[3]

$$\epsilon_R = K_1 \frac{a}{R} = K_1 \sin\gamma \quad . \tag{5}$$

Here, K_1 is about 0.2 and γ is a contact angle between the indenter and the specimen as shown in Fig. 3. This equation is based on the experimental results obtained using the traditional optical technique. A similar definition has also been proposed by considering the work-hardening characteristics;[18] $\epsilon_R = 0.28\,(1 + 1/n)^{-n}\, a/R$, where the constant corresponding to K_1 varies slightly from 0.17 to 0.19.

Second, ϵ_R can be defined as the average shear strain using the relation[7,9,20]

$$\epsilon_R = K_2 \frac{h_c}{a} \quad . \tag{6}$$

This equation can also be derived from Eq. (5) using the relation $a^2 \approx 2Rh_c$ for shallow indentation, and K_2 is about 0.4.

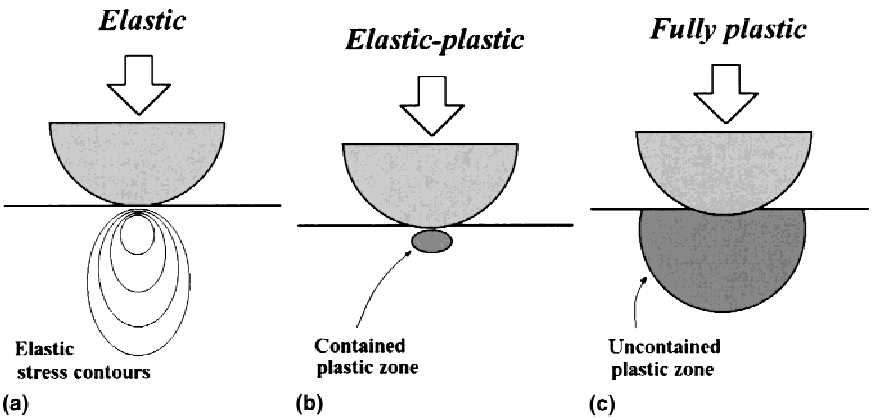

FIG. 1. Schematic representation of plastic zone expansion during ball indentation: (a) elastic, (b) elastic–plastic, and (c) fully plastic regimes.[9]

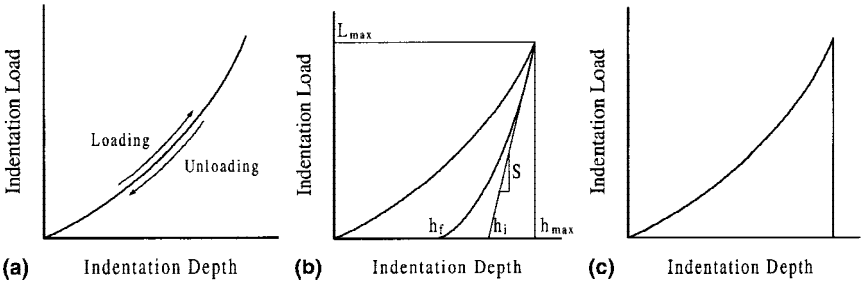

FIG. 2. Typical indentation load–depth curves for (a) elastic, (b) elastic–plastic, and (c) plastic responses.

Third, ϵ_R can be defined as the average plastic strain in depth direction by analyzing the area change during indentation. For the fully plastic regime where the elastic deformation is negligible, the average strain in depth direction can be obtained as

$$\epsilon_{zz} = -(\epsilon_{xx} + \epsilon_{yy}) = -\int_{S1}^{S2} \frac{dS}{S} = \ln \frac{S1}{S2} \quad , \qquad (7)$$

where $S1$ is the initial area (projected contact area) and $S2$ is the area changed by indentation (curved contact area) shown in Fig. 3. Since $S1 = \pi a^2$ and $S2 = 2\pi R^2 (1 - \cos\gamma)$,

$$\epsilon_R = -\epsilon_{zz} = \ln \frac{2}{1 + \cos\gamma} \quad . \qquad (8)$$

This definition of strain has the advantage of not needing an ambiguous constant compared with the widely used definitions of strain such as Eqs. (5) and (6). As a comparison with Eq. (8), for a Vickers indenter, ϵ_R is constant regardless of indentation depth, i.e., $\epsilon_R = -\ln\cos\gamma \approx 0.076$.[21]

Finally, the strain distribution under the indenter can be calculated using the displacement in depth direction u_z. For a ball indenter,

$$u_z = h - \left(R - \sqrt{R^2 - r^2}\right) \quad , \qquad (9)$$

By differentiating,

$$\epsilon_{zr} = \frac{\partial u_z}{\partial r} = -\frac{1}{\sqrt{1 - (r/R)^2}} \frac{a}{R} \quad . \qquad (10)$$

This strain distribution is a first approximation because the pressure distribution for elastic–plastic deformation of materials with work-hardening deviates significantly from the Hertzian.[19] ϵ_R can then be defined by setting $r = a$ and multiplying a constant α:

$$\epsilon_R = \frac{\alpha}{\sqrt{1 - (a/R)^2}} \frac{a}{R} = \alpha \tan\gamma \quad . \qquad (11)$$

Here, $\tan\gamma$ is the shear strain at contact edge and α is expected to be a material-independent constant. This is because the average strain is determined by the amount of geometrical change due to external loading like Eq. (8), although its local values can vary significantly with position. Accordingly, we determine this constant using the experimental results on various steels to result in a good match between ϵ_R and σ_R.

Next, the representative stress σ_R can be obtained from the mean contact pressure P_m. In the elastic regime, the value of P_m/σ_R ratio increases linearly up to about 1.1. It increases gradually through the elastic–plastic regime and is almost constant in the fully plastic regime:[3,9]

$$P_m/\sigma_R = \Psi \quad . \qquad (12)$$

Here Ψ is expected to have some relationship with plastic-zone expansion, i.e., the yield strain and the work-hardening exponent. The upper value of Ψ is about 3 for the fully plastic deformation.[22]

III. EXPERIMENTAL PROCEDURE

The specimens used in this study were AISI1025, SA106, SA213, SA508, SM50, and TMCP steels; their compositions are summarized in Table I. Specimen dimension for indentation testing was 20 × 20 × 15 mm. Specimen surface was finally polished with 1 μm Al_2O_3 powder. In addition, the specimen for the tensile test was fabricated as a cylinder type with 25-mm gauge length and 6-mm diameter.

A continuous indentation tester was made to measure the indentation load–depth curve. It consists of a 500-kgf loadcell and a linear variable displacement transducer (LVDT) with resolution of 0.2 μm. To minimize the error caused by system compliance, the indenter and LVDT were placed as closely together as possible. The indenter was a W ball of 0.5-mm radius, and indentation speed was 0.1 mm/min. The final maximum depth was 0.3 mm and 10 partial unloadings down to 70% of maximum load at each point were applied. More than five indentations per specimen were performed to examine reproducibility. For verification of our analysis, true stress–true strain curves for various steels were directly measured by tensile tests at cross-head speed of 1 or 2 mm/min.

IV. RESULTS

The measured indentation load–depth (P-h) curves of AISI1025, SA106, SA213, SA508, SM50, and TMCP steels are shown in Fig. 4. For each specimen, more than 5 curves were measured; reproducibility was excellent within 3% load error range at each depth. Although the results from all P-h curves for each specimen make little difference, the one with the highest load at each indentation depth was chosen and analyzed to minimize the

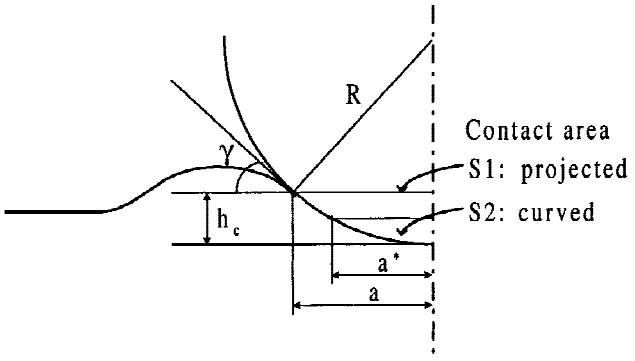

FIG. 3. Schematic representation of pileup phenomenon.

TABLE I. Chemical compositions of materials used in this study (wt%).

Materials	C	Mn	Si	Al	Ni	Cr	Mo	P	S
AISI1025	0.24	0.44	0.24	⋯	0.2	0.1	0.01	0.003	0.003
SA106	0.26	1.18	0.2	⋯	0.09	0.11	0.04	0.007	0.001
SA213	0.12	0.47	0.38	⋯	0.35	2.3	1	0.008	0.001
SA508	0.21	1.36	0.24	0.022	0.92	0.21	0.49	0.007	0.002
SM50	0.18	1.31	0.4	⋯	0.02	0.11	⋯	0.011	0.038
TMCP	0.138	1.2	0.23	⋯	0.002	0.002	⋯	0.017	0.001

error caused by the effect of sliding at initial loading or surface roughness. As shown in Fig. 4, SA508 steel shows the highest resistance to penetration and AISI1025 steel the lowest.

The commencement of plastic deformation, i.e., the boundary between the elastic regime and the elastic–plastic regime for each specimen, was not detected in the indentation load–depth curve measured in our experiments. The critical indentation load for the initial plastic deformation P_Y during ball indentation is obtained as[22]

$$P_Y = \frac{\pi^3 R^2}{6E_r^2} (\tfrac{1}{2} P_m)^3 \quad , \tag{13}$$

where E_r is the reduced modulus with relation $1/E_r = (1 - n_2)/E + (1 - ni_2)/E_i$, and P_m is equal to 1.1 times the yield strength Y at the initial plastic deformation. E and ν are the elastic modulus and the Poisson ratio of specimen, respectively, and subscript i means the indenter. For example, the value of P_Y for AISI1025 steel is calculated as 0.2 gf by setting $E = 160$ GPa, $\nu = 0.3$, $E_i = 400$ GPa, $\nu_i = 0.28$, $R = 0.5$ mm, and $Y = 196$ MPa, which is too low to be detected in our indentation system.

The boundary between the elastic–plastic regime and the fully plastic regime is determined by a nondimensional variable $E_r/Y \cdot \tan\gamma$, and the value of $E_r/Y \cdot \tan\gamma$ is about 30.[22] In our study, the value of $E_r/Y \cdot \tan\gamma$ was calculated as more than about 100 for all specimens, so the following procedure was used to determine the plastic flow properties of specimens from the measured indentation load–depth curve.

In analyzing the measured *P-h* curves, we first calculated the elastic deflection at each indentation step. The unloading curve follows the equation[16]

$$P = k(h - h_f)^l \quad , \tag{14}$$

where k and l are material constants and h_f is the final depth. By differentiating P with h and putting $h = h_{max}$, we obtained the stiffness and then calculated the elastic deflection depth.

To consider the change of contact area due to pileup or sink-in, the work-hardening exponent n was calculated using the iteration method. By assuming an initial value of n as 0.3, we could obtain the true stress–true strain (σ_R-ϵ_R) relation through the analysis proposed in Sec.II.B. Then the value of n was modified using the Hollomon equation $\sigma_R = K\epsilon_R^n$ with fitting range of $\epsilon_R < n$. This fitting range is based on the fact that the strain at maximum load in the uniaxial tensile test is equal to n. Through iteration this procedure until the input value equaled the return value, the final value of n was achieved.

The flow properties derived from indentation load–depth curve and those measured by tensile test are shown together in Fig. 5. The constant α in Eq. (11) was found to be 0.1, showing the best agreement between them. In this figure, we first examined the work-hardening characteristics for the proposed definitions of strain in Sec.II.B: $0.2\sin\gamma$, $0.4h_c/a$, $\ln[2/(1 + \cos\gamma)]$, and $0.1\tan\gamma$. Then the effects of pileup or sink-in on the derivation of stress–strain relationship were investigated.

The best agreement between the true stress–true strain data derived from ball indentations and those measured by tensile tests was achieved when we defined the strain in indentation as $0.1\tan\gamma$. In other words, the shear strain at contact edge multiplied by 0.1 successfully predicted the work-hardening characteristics of the proposed materials with various n, shown in Fig. 6. So the bulk properties from the stress–strain data derived from ball indentations could be predicted, the stress–strain data where the flow stress decreases with increasing strain were excluded in fitting these data to the Hollomon equation, especially for SA508 steel.

The strain definitions in terms of a/R and h_c/a show the similar trend in deriving n from ball indentations and have large deviations from tensile results. In the case of strain definition as an average plastic strain in depth-direction, i.e., $\ln[2/(1 + \cos\gamma)]$, the values of work-hardening exponent derived from indentation are lower than the tensile data, shown in Fig. 6, while this definition of strain has the advantage of not needing an experimentally determined constant.

The pileup or sink-in caused mainly by work-hardening characteristics has a strong effect on calculating the absolute values of strain and stress in indentation. If the pileup occurs for the material with low n, the contact radius increases, so the strain increases and the stress decreases, shown in Fig. 5. This effect is clearly shown in Fig. 7 by investigating the variations of P_m/σ_R ratio with n. It is seen that the value of P_m/σ_R ratio is

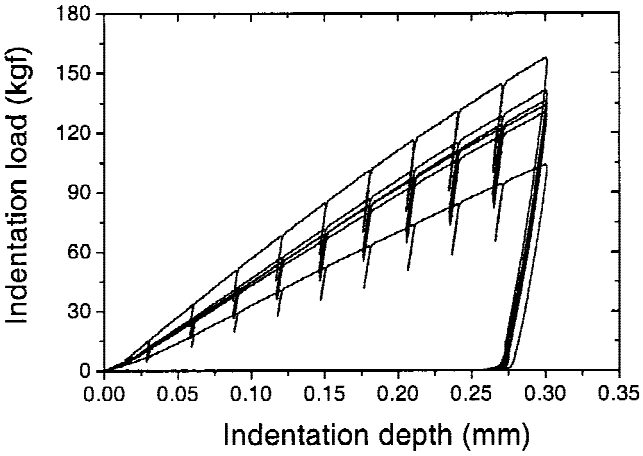

FIG. 4. Measured indentation load–depth curves of SA508, TMCP, SA106, SA213, SM50, and AISI1025 steels in the order of higher load value at depth of 0.3 mm.

almost constant only when the pileup/sink-in behavior is taken into account; it varies significantly between 2.6 and 3.4 in other cases.

The result of $P_m/\sigma_R \approx 3$ for steels in our study agrees well with the results obtained from the traditional optical method of residual imprint,[3,9] and those from finite element work.[19] In addition, this result also satisfies the fact that the upper value of the P_m/σ_R ratio is about 3 for the fully plastic deformation.[22] If this simple relation is valid for various steels, the usefulness of indentation as a substitute for tensile testing will be greatly improved. Accordingly, the incorporation of pileup/sink-in effects is essential in determining the real contact between the indenter and the specimen from the indentation load–depth curve.

V. DISCUSSION

Looking into some important current research on derivation of stress–strain relationship from indentations, we found that Field and Swain[11] performed nanoindentation experiments with carefully calibrated spheroconical indenters with tip radii of 5 and 10 μm. They considered the pileup/sink-in by estimating the work-hardening exponent, which was calculated by the relation $P \propto a^{*(2+n)}$. This relation was derived from Meyer's law[23] $P = Ka^m$ and the fact that $m = n + 2$,[3] where K is a material constant and m is a hardening factor. Alcalá *et al.*[13] calculated Young's modulus within an elastic regime using an macroindenter with better sensitivity than our indenter. They estimated the yield strength and work-hardening exponent in the fully plastic regime. The work-hardening exponent was calculated by the relation $P \propto h^{1+(n/2)}$. This relation was also derived from Meyer's law[23] and the fact that $m = n + 2$.[3] Taljat *et al.*[14] derived the stress–strain curve by finite element analysis. They defined stress and strain at maximum and minimum strain points to obtain a wide range of stress–strain curves.

In our study, a new strain definition of $0.1\tan\gamma$ instead of the commonly used $0.2\sin\gamma$[3] and $0.4h_c/a$[7,9,20] is suggested, which results in the best agreement between the stress–strain curves derived from ball indentations and those measured directly by tensile tests. It is clearly shown that the effects of elastic deflection and pileup/sink-in must be included at the same time in determining the real contact area, as suggested by Field and Swain,[11] by investigating the value of the P_m/σ_R ratio. The work-hardening exponent is derived by the iteration method as a parameter to determine the pileup/sink-in, not by Meyer's law. In summary, our theoretical analysis and systematic experiments provide new and precise technique to derive the plastic stress–strain relationships of steels with different work-hardening characteristics. A drawback of this technique is that the elastic modulus calculated from the unloading curve[15,16] is underestimated, possibly due to extremely large plastic deformation in our experiments. In addition, the method[13] of analyzing the elastic response in Hertzian regime cannot be applied for these materials. It is shown that the critical indentation load for the initial plastic deformation is on the 0.1 gf order for these steels, which is too low to be detected in our indentation system.

The effect of anisotropy and texture can be significant in evaluating the mechanical properties of steels, and it must be taken into account in developing the theoretical analysis. This effect is very complicated due to the complex stress fields beneath the ball indenter, so further study is required. However, the effect of anisotropy and texture was negligible in our experiments since the specimens were the commercial steels with large volume. And, the variation of properties with depth was carefully considered by keeping the indentation and tension samples at the same position especially for SA508 steel.

The shape and size of plastic zone developed beneath the indenter are mainly dependent on the yield strain ϵ_Y and the work-hardening exponent n. For materials with small ϵ_Y and n, the plastic zone will expand well to the surface around indentation. It is thus expected that the pileup of these materials beneath the indenter will be larger than those of materials with large ϵ_Y and n at the same depth. For various steels in this study, the yield strain is very small and can be regarded as the same (0.001–0.003) while it must be taken into account for materials with large yield strain such as glass, ceramics or rubber. Hence, it is reasonable to determine the extent of pileup/sink-in using only n as in Eq. (3).

The work-hardening exponent derived from indentation load–depth curve n_{ind} is, however, somewhat different from that measured by tensile test n_{ten}. One

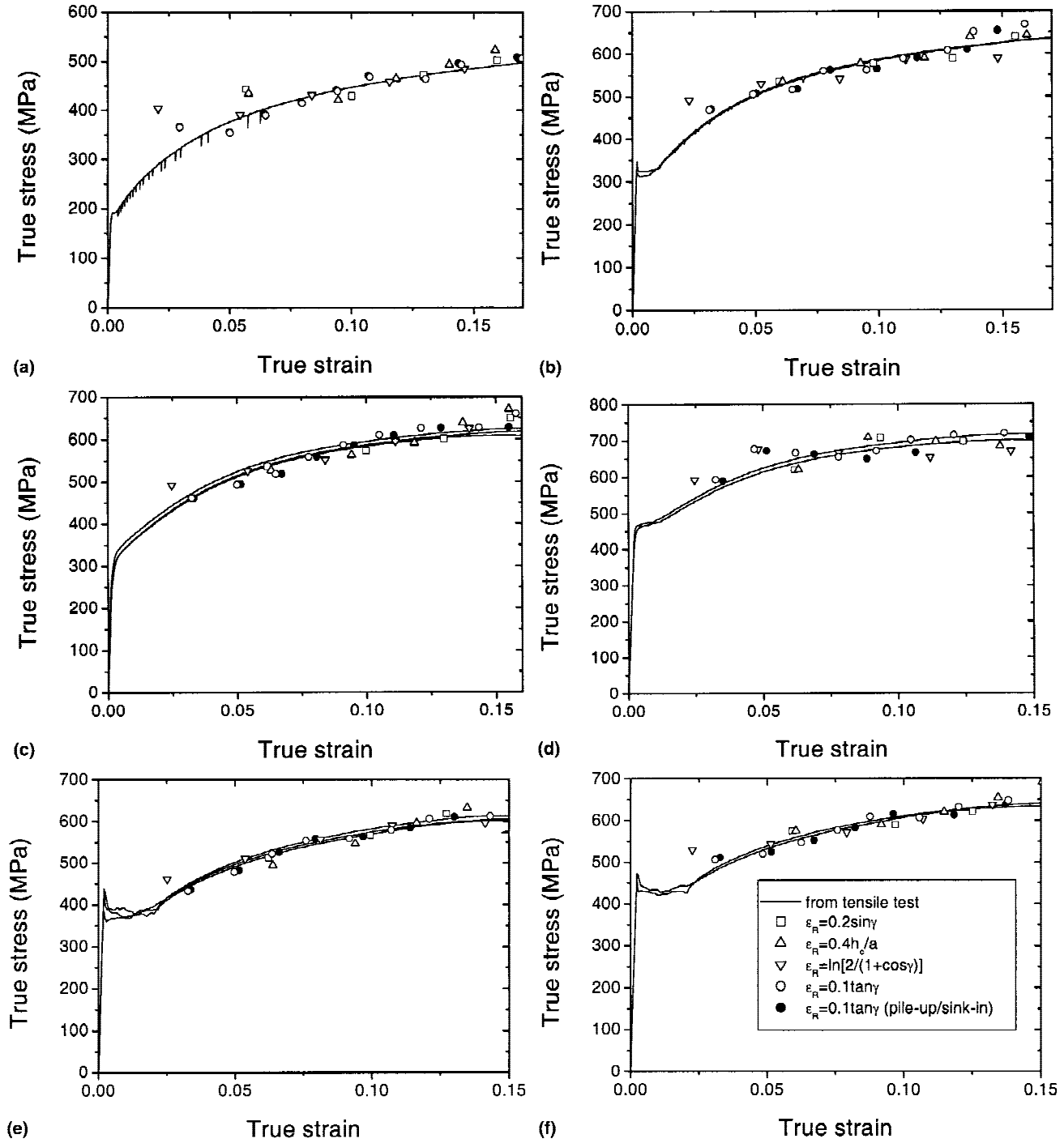

FIG. 5. Comparisons between flow properties calculated from the continuous indentation test and those from the tensile test for (a) AISI1025, (b) SA106, (c) SA213, (d) SA508, (e) SM50, and (f) TMCP steels.

difference is that the value of n_{ind} is available in strain range more than 0.03 in our study while n_{ten} is obtained using true stress–true strain data from the yielding point. Another is that surface properties might vary from bulk properties. For example, if the surface of the specimen is work-hardened, the value of n_{ind} will be lower than that of n_{ten}. Then, n_{ind} is more appropriate for determining the extent of pileup/sink-in. This is because indentation itself is a surface-proving technique and the plastic deformation during indentation will be much more severe than in tension.

As mentioned previously, the indentation technique is largely affected by the surface properties of materials. For some steels such as AISI1025 and SA508, the flow

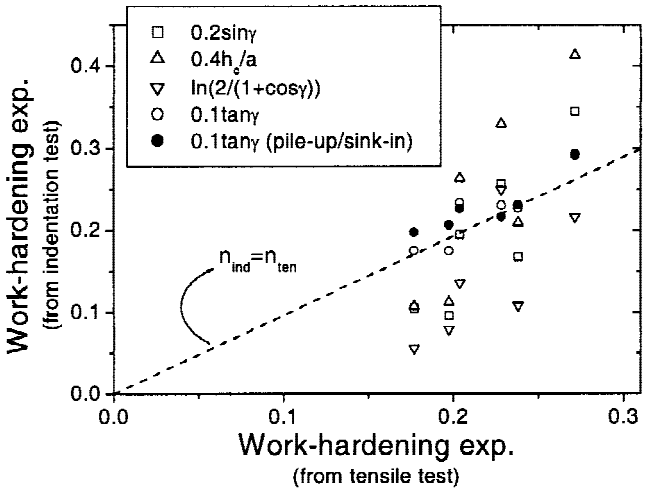

FIG. 6. Comparison between the work-hardening exponent derived from ball indentations and that measured by the tensile test; the stress–strain data where the flow stress decreases with increasing strain were excluded in deriving the work-hardening exponent from ball indentations, especially for SA508 steel.

stress decreases with increasing strain at initial stage, perhaps due to the indenting of hardened surface. In this case, care must be taken when the experimental data is analyzed. For example, we must define the useful data range (Fig. 6) or predict bulk properties by measuring the depth profile of mechanical properties through cross-sectional indentation. To find out the yield strength from the indentation load–depth curve, it may be more reliable to extrapolate the yield strength from the useful σ_R-ϵ_R data than to measure the initial yielding point and calculate the yield strength; the curve excursions resulting from the indenting of surface oxide layer[24] or

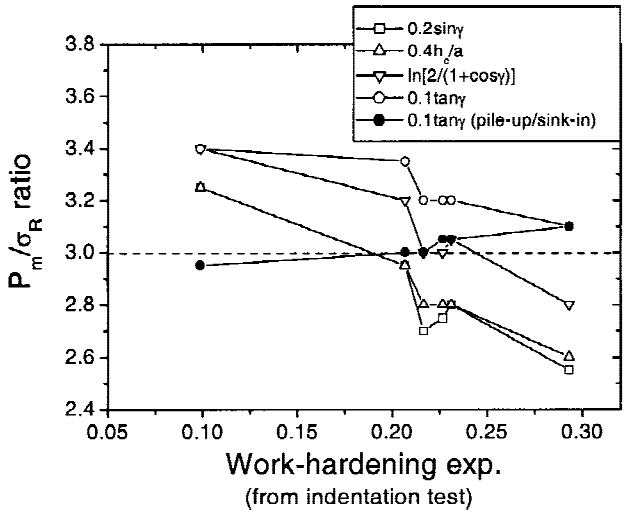

FIG. 7. The relationship between P_m/σ_R ratio and work-hardening exponent derived from ball indentations; all the stress–strain data in Fig. 5 were included in deriving the work-hardening exponent from ball indentations.

the dislocation nucleation and/or movement[25] at initial loading complicate the interpretation of the indentation load–depth curve measured at initial yielding.

VI. CONCLUSIONS

Plastic flow properties of various steels were evaluated from the load–depth curve measured by ball indentation. (1) The contact radius was determined from the indentation load–depth curve. Then the elastic deflection was obtained by analysis of the unloading curve. The effect of pileup/sink-in was incorporated using the work-hardening exponent. (2) Various definitions of representative strain were attempted: $0.2\sin\gamma$, $0.4h_c/a$, $\ln[2/(1+\cos\gamma)]$, and $0.1\tan\gamma$. As a result, the shear strain at contact edge was proved to be the best expression for the work-hardening characteristics of materials. (3) The value of the P_m/σ_R ratio was almost constant, about 3, when the effect of pileup/sink-in was considered. This agrees well with the results from the traditional optical method of residual imprint, which makes our analysis very powerful. (4) Flow properties derived from indentation load–depth curve were in good agreement with those measured by tensile test for various steels such as AISI1025, SA106, SA213, SA508, SM50, and TMCP. (5) The ball indentation technique was proved to be an excellent substitute for the standard tensile test; it has the potential to be applied nondestructively to evaluate the mechanical properties of small volumes such as welds and heat-affected zones.

REFERENCES

1. S.P. Baker and T.P. Weihs, in *Thin Films: Stresses and Mechanical Properties IV*, edited by P.H. Townsend, T.P. Weihs, J.E. Sanchez, Jr., P. Børgesen (Mater. Res. Soc. Symp. Proc. **308,** Pittsburgh, PA, 1993), p. 217.
2. J. Menčík and M.V. Swain, Mater. Forum **18,** 277 (1994).
3. D. Tabor, *The Hardness of Metals* (Clarendon Press, Oxford, United Kingdom, 1951).
4. D.M. Marsh, Proc. R. Soc. London, Ser. A **279,** 420 (1964).
5. C-H. Mok, Exp. Mech. **Feb,** 87 (1966).
6. R.A. George, S. Dinda, and A.S. Kasper, Met. Progress **May,** 30 (1976).
7. D. Kramer, H. Huang, M. Kriese, J. Robach, J. Nelson, A. Wright, D. Bahr, and W.W. Gerberich, Acta Mater. **47,** 333 (1999).
8. J.H. Underwood, G.P. O'Hara, and J.J. Zalinka, Exp. Mech. **Dec,** 379 (1986).
9. H.A. Francis, Trans. ASME (Series H) **9,** 272 (1976).
10. F.M. Haggag, in *Small Specimen Test Techniques Applied to Nuclear Reactor Vessel Thermal Annealing and Plant Life Extension*, edited by W.R. Corwin, F.M. Haggag, and W.L. Server (American Society for Testing and Materials, Philadelphia, PA, 1993), pp. 27–44.
11. J.S. Field and M.V. Swain, J. Mater. Res. **10,** 101 (1995).
12. A.C. Fischer-Cripps and B.R. Lawn, Acta Mater. **44,** 519 (1996).
13. J. Alcalá, A.E. Giannakopoulos, and S. Suresh, J. Mater. Res. **13,** 1390 (1998).
14. B. Taljat, T. Zacharia, and F. Kosel, Int. J. Solids Structures **35,** 4411 (1998).
15. M.F. Doerner and W.D. Nix, J. Mater. Res. **1,** 601 (1986).

16. W.C. Oliver and G.M. Pharr, J. Mater. Res. **7,** 1564 (1992).
17. I.N. Sneddon, Int. J. Eng. Sci. **3,** 47 (1965).
18. J.R. Mattews, Acta Metall. **28,** 311 (1980).
19. R. Hill, F.R.S., B. Storåkers, and A.B. Zdunek, Proc. R. Soc. London, Ser. A **423,** 301 (1989).
20. K.L. Johnson, J. Mech. Phys. Solids **18,** 115 (1970).
21. Yu.V. Milman, B.A. Galanov, and S.I. Chugunova, Acta Metall. Mater. **41,** 2523 (1993).
22. K.L. Johnson, *Contact Mechanics* (Cambridge University Press, Cambridge, United Kingdom, 1985).
23. E. Meyer, Z. ver. Deutshe Ing. **52,** 645 (1908).
24. W.W. Gerberich, S.K. Venkataraman, H. Huang, S.E. Harvey, and D.L. Kohlstedt, Acta Metall. Mater. **43,** 1569 (1995).
25. A.B. Mann and J.B. Pethica, in *Thin Films: Stresses and Mechanical Properties VI*, edited by W.W. Gerberich, H. Gao, J-E. Sundgren, and S.P. Baker (Mater. Res. Soc. Symp. Proc. **436,** Pittsburgh, PA, 1997), p. 153.